

The Effect of Jet-Streak Curvature on Kinematic Fields

JAMES T. MOORE

Saint Louis University, Department of Earth and Atmospheric Sciences, St. Louis, Missouri

GLENN E. VANKNOWE

Staff Meteorology Office, Rome Laboratory, Griffiss Air Force Base, New York

(Manuscript received 1 March 1991, in final form 4 February 1992)

ABSTRACT

A simple two-layer primitive equation (PE) model is used to study the effect of curvature on jet-streak kinematics, specifically vertical motion. Three types of vertical motion are studied: kinematic (PE) vertical motion, quasigeostrophic (QG) vertical motion, and vertical motion associated with an unbalanced component of the flow, partially due to inertial-gravity waves (IGW). The latter vertical motion is computed as the difference between the PE vertical motion and "balanced" vertical motion derived from Krishnamurti's balanced omega equation. In addition, the upper-level ageostrophic flow is discussed as it relates to the patterns of divergence associated with various jet curvatures. The PE model was run out to 12 h to see how straight-line (SL), cyclonic (CY), and anticyclonic (AC) curvature affects jet-streak kinematics.

At the initial time, a two-cell pattern of vertical motion was found for the CY and AC jet streaks as opposed to the four-cell pattern associated with the SL jet streak. Also, the vertical-motion centers for the AC and CY jet streaks were aligned more along the jet axis than across it, in contrast with the SL case. Quasigeostrophic vertical motion for the SL and CY jet cases agreed well with the PE vertical motion but were much weaker than the PE vertical motion for the AC case.

Results for 12 h into the model run showed that unbalanced or IGW vertical motions were strongest for the CY case where they were equal to about one-half of the PE vertical motions. A comparison of QG vertical motion with balanced vertical motion illustrates the effect of curvature most dramatically. For cyclonic curvature, QG vertical motions are 50% stronger than the balanced vertical motions, while for anticyclonic curvature, they are 50% weaker than the balanced vertical motion. For the SL and AC cases, unbalanced vertical motions were smaller but were still a significant part of the total PE vertical motion. Thus, the greatest mutual adjustment between the mass and momentum fields occurs with cyclonically curved jet streaks. A comparison of vertical motions from runs in which the curvature was varied revealed that the magnitude of the vertical motion is strongest with cyclonic jet streaks, more modest with anticyclonic jet streaks, and weakest with straight-line jet streaks. This is reflected in the maximum Rossby numbers for these cases that were 1.0, 0.40, and 0.12, respectively.

1. Introduction

The kinematic fields associated with straight-line and curved jet streaks have been discussed by several researchers. Beebe and Bates (1955) have described the typical vertical motion and divergence patterns for upper-level jet streaks of varying curvature. For a westerly upper-level jet streak (see Fig. 1a), the entrance region is upstream of the jet core and the exit region is downstream from the jet core. Looking downstream in the Northern Hemisphere, left is to the north and right is to the south. In the straight-line jet-streak case, a four-cell pattern of divergence-convergence is expected, with divergence in the left-exit and right-entrance quadrants and convergence in the right-exit and left-

entrance quadrants. For cyclonically curved jets, Beebe and Bates (1955) showed that the divergence-convergence quadrants on the cyclonic side of the jet are enhanced, while the two anticyclonic quadrants' divergence-convergence are quantitatively ill defined. The opposite is true for anticyclonically curved jets. Upward (downward) vertical motion at midlevels will generally accompany upper-level divergence (convergence).

More recently, Keyser and Shapiro (1986) described the divergence-convergence fields attending straight-line and curved jet streaks in terms of their along- and cross-contour ageostrophic wind fields (Figs. 1a,b). For a straight-line jet streak, the cross-contour ageostrophic wind dominates, creating the four-cell pattern described earlier that has been emphasized, perhaps too much so, in the literature (Fig. 1a). The effect of cyclonic curvature on a uniform flow is to enhance divergence east of the trough and convergence west of the trough (Fig. 1b); this is due to the along-contour component of the ageostrophic wind. One can see that superim-

Corresponding author address: Dr. James T. Moore, Saint Louis University, Department of Earth and Atmospheric Sciences, 3507 Laclede Ave., Saint Louis, MO 63103.

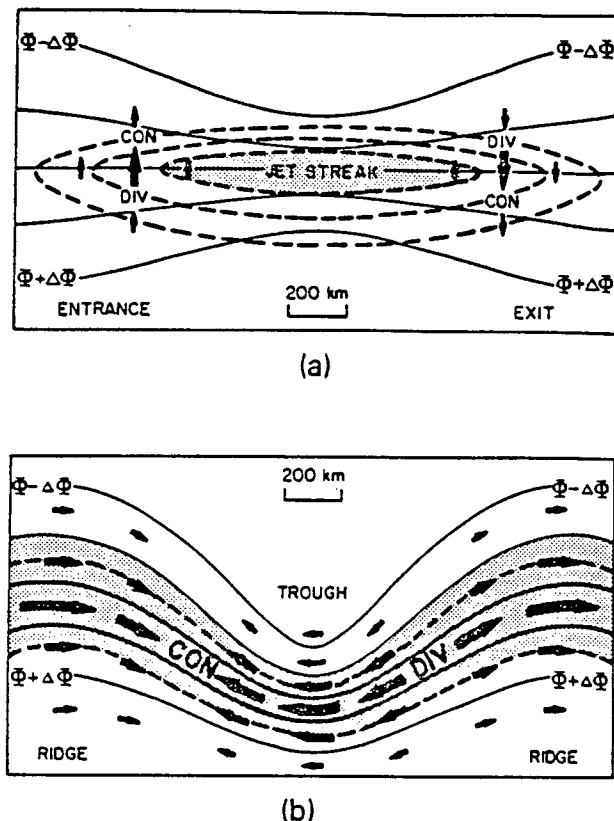


FIG. 1. Schematic representation of the ageostrophic motions (heavy arrows) and associated patterns of convergence (CON) and divergence (DIV) in the vicinity of (a) a straight jet streak in the absence of along-contour thermal advection and (b) a uniform jet streak within a stationary synoptic-scale wave. Both representations are assumed to apply at or near the level of maximum wind, where the horizontal wind distribution is most distinct and the flow is approximately horizontal. Solid lines indicate geopotential height of a constant-pressure surface; dashed lines are isotachs (maximum wind speed shaded). Adapted from Shapiro and Kennedy (1981).

posing the two ageostrophic flows in Fig. 1a,b would create strong divergence–convergence centers on the cyclonic side of the jet; the sign of the divergence on the anticyclonic side of the jet depends on the relative strength of the along- versus cross-stream ageostrophic wind components. Just the opposite conditions would take place for anticyclonically curved flow. These concepts agree with the Beebe and Bates (1955) model while emphasizing the ageostrophic flow due to curvature of the baroclinic wave and the effect of the along-stream variation in wind speed. Yet, both sets of authors provide no quantitative verification of these physical models using either observed or model-simulated data. However, Cammas and Ramond (1989) have used numerical analyses from the European Centre for Medium-Range Weather Forecasts (ECMWF) to diagnose along- and cross-stream ageostrophic wind components in the entrance and exit regions of two jet streaks within a baroclinic wave.

Analyses from three case studies document that curvature effects can contribute in a predominant way to the ageostrophic divergence in both entrance and exit regions of jet streaks. In some cases the curvature effect can even inhibit the expected transverse circulations associated with these regions.

Houghton et al. (1981) and Van Tuyl and Young (1982) developed a simple primitive equation (PE) model to simulate kinematic fields associated with upper-level jet streaks. Van Tuyl and Young (1982) explored the patterns of vertical motion for straight-line jet streaks associated with various magnitudes of velocity. They noted that the classical four-cell pattern of vertical motion was still pronounced after 12 h with a 26 m s^{-1} jet streak (Rossby number = 0.26). However, after 12 h, the 39 and 52 m s^{-1} jet streaks (Rossby numbers = 0.39 and 0.52, respectively) developed a three-cell vertical motion pattern with a dominant upward vertical-motion (UVM) center upstream from the jet core and two downward vertical-motion (DVM) centers on either side along the jet axis.

In this paper, the same PE model developed by the above researchers is used to study the effects of curvature on the kinematic fields accompanying a moderate jet streak. Section 2 describes the PE model and the kinematic fields to be evaluated, including quasi-geostrophic (QG), “balanced,” and “actual” vertical motion, the latter being based on the model divergence fields. This PE model also permits evaluation of the unbalanced or inertial-gravity wave (IGW) vertical-motion contribution, which is a function of the curvature of the jet streak and the maximum wind speed in the jet core.

Section 3 displays the results of these calculations for straight-line (SL), cyclonically (CY) curved, and anticyclonically (AC) curved jet streaks. Finally, section 4 will summarize the impact of our findings concerning vertical motion approximations associated with various curvatures of jet streaks.

2. Description of the model and kinematic fields

a. The PE model

To study the effect of curvature, a PE model developed by Houghton et al. (1981) and Van Tuyl and Young (1982) was adapted to account for jet-streak curvature. The only change was to add the effect of curvature to the initial ψ field. The modification was made to Van Tuyl and Young’s (1982) specification of ψ as follows:

$$Y = y + \left\{ 1 - \cos \left[\left(\frac{\pi}{h} \right) \left(\frac{h}{2} - |x| \right) \right] \right\} \times \left(\frac{D-y}{D} \right)_{AC} \quad (1)$$

$$L(x) = a - b \cos(2\pi h^{-1}x) \quad (2)$$

$$\psi_{800} = \Psi_{800} \left\{ \frac{\tan^{-1}[Y/L(X)]}{\tan^{-1}[D/L(X)]} \right\} \quad (3)$$

$$\psi_{400} = 3\psi_{800}, \quad (4)$$

where x and y are grid coordinates, $h = 4000$ km, $a = 833.3$ km, $b = 458.3$ km, $D = 1900$ km, A is the amplitude (km) of the trough or ridge (770 km in this case), C is the type of curvature (1 = cyclonic, 0 = straight line, -1 = anticyclonic), and Ψ_{800} is the streamfunction amplitude ($7.0 \times 10^6 \text{ m}^2 \text{ s}^{-1}$ for SL case; $5 \times 10^6 \text{ m}^2 \text{ s}^{-1}$ for CY and AC cases). These above equations were applied to a 25 (X axis) \times 21 (Y axis) grid with zero at the center. Although the computational grid was 25 \times 21, a display grid of 21 (X axis) \times 19 (Y axis) was chosen. On the display grid, the point $x = 0, y = 0$ is found at grid location $i = 10.5, j = 9.5$, where i is the column indicator and j is the row indicator of the grid system. A Cartesian coordinate system was used such that x increases to the east and y increases to the north. The steps that follow are described in detail by Houghton et al. (1981, 2119–2121) and Van Tuyl and Young (1982, 2040–2041). Once the streamfunction has been specified for the two model levels (800 and 400 mb; see Fig. 2), the geopotential is obtained by solving the “reverse” balance equation. These heights are then linearly extrapolated to 1000 and 200 mb and interpolated to 600 mb. The initial vertical motion field at 600 mb is determined by the balanced omega equation of Krishnamurti (1968), as described by Houghton et al. (1981). Thereafter, ver-

tical motion is computed through downward integration of the continuity equation. In this paper, these kinematic vertical motions will be known as the PE vertical motion and are valid at 600 mb. The model is adiabatic, hydrostatic, contains no friction, and uses a constant Coriolis parameter (10^{-4} s^{-1}) over the 4800-km \times 4000-km grid (grid distance is 200 km). Boundary conditions were periodic in x , and the v component of the wind was set equal to zero at the channel walls. Thus, our simplified jet streak is set in an east–west channel and does *not* interact with other jet streaks as is often seen in the real atmosphere. This does limit the generality of our results.

The jet streaks that will be discussed have core wind speeds of 36.0, 34.2, and 35.6 m s^{-1} for the SL, CY, and AC cases, respectively. This selection was based as closely as possible on the middle case that Van Tuyl and Young (1982) studied. The model was run out only to 12 h since the major kinematic features were present by that time. All resultant fields were plotted after being passed through a Shuman (1957) smoother of 0.2, which reduced numerical noise. The Shuman nine-point smoother can be set from 0.1 to 0.9, so a smoother of 0.2 chosen for this study is relatively small.

b. Kinematic fields

Typically, a qualitative estimate of the vertical motion pattern can be obtained by identifying regions of low–middle-level warm-air advection and/or middle–upper-level positive vorticity advection. Essentially, these “rules” result from the (sometimes loose) application of quasigeostrophic (QG) theory (Holton 1979). Models of the secondary direct (indirect) thermal circulations in the entrance (exit) regions of jet streaks described by Beebe and Bates (1955) and Uccellini and Johnson (1979) also provide qualitative examples for guidance in estimating vertical motion.

Presently, however, one of the few quantitative means for diagnosing vertical motion in an operational environment in real time is through the **Q**-vector diagnostics program developed by Barnes (1985, 1987). Basically, **Q** vectors can be computed using only the height field on three constant-pressure surfaces and replacing the right-hand side of the standard QG omega equation with one term, namely the divergence of the **Q** vector. Although this QG diagnosis of vertical motion (actually *implied* by the **Q**-vector divergence pattern) is quite helpful for understanding the large-scale forcing of vertical motion, it can have its shortcomings, especially in the presence of significant curvature in the jet streak when centrifugal forces play a crucial role in the dynamics of the airflow. The **Q**-vector diagnostics are essentially a means for quantifying the geostrophic adjustment processes, in this case, associated with jet-streak propagation. In this sense, it is not only the curvature of the jet streak that is important to the geostrophic adjustment process, but also the magnitude

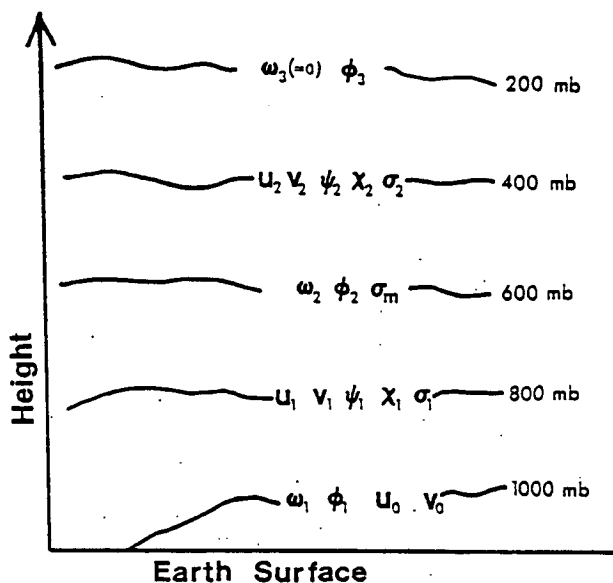


FIG. 2. Vertical structure and placement of variables in the model (Houghton et al. 1981). Variables are as follows: ω = vertical motion, ϕ = geopotential, ψ = streamfunction, χ = velocity potential, u and v = horizontal wind components, and σ = static stability.

of the subsequent ageostrophic motions and the rate at which they develop. The \mathbf{Q} -vector diagnostics will generally not yield a reasonable estimate of the vertical motions due to geostrophic adjustment when the resulting ageostrophic motions change rapidly or reach large magnitudes. This is especially important, for instance, as a jet streak propagates around the base of a long-wave trough and undergoes changes in curvature.

Vertical motion can also be computed diagnostically using a modified form of Krishnamurti's (1968) balanced omega equation as discussed by Houghton et al. (1981). In this modified form, terms 1, 2, 3, 4, and 10 of Krishnamurti's original 12 terms are retained; the other terms are neglected on the basis of scale analysis and model approximations. Terms 1, 2, 3, 4, and 10 of Krishnamurti's balanced omega equation include the following: differential vorticity advection by the nondivergent part of the wind, Laplacian of the thermal advection by the nondivergent part of the wind, the differential deformation term, the vertical differential divergence effects term, and the differential advection of vorticity by the divergent wind. The terms that were neglected include the effects of frictional stress, latent and sensible heat, differential vertical advection of vorticity, differential turning of vortex tubes, Laplacian of thermal advection by the divergent wind, and a beta term. The terms neglected or retained follow the work of Houghton et al. (1981) in computing a "balanced" vertical motion. The "balanced" vertical motions include more forcing terms than QG forcing, and therefore one would expect them to closer approximate the actual vertical motion. However, balanced vertical motions are not typically available in the operational setting due to limited computational resources.

Houghton et al. (1981) describe how unbalanced vertical motions can be diagnosed in this model by subtracting the balanced vertical motion from the PE kinematic vertical motion; the latter are based on the model-generated divergence-convergence. Houghton et al. (1981) denoted these unbalanced vertical motions as those vertical motions that are due to the presence of IGWs. Although it is possible that the unbalanced vertical motion could be the result of processes other than those associated with IGWs, we will term them *IGW vertical motion*. In the next section, QG, PE, and IGW vertical motions will be displayed for each of the three jet streaks (SL, CY, and AC). The ageostrophic wind vectors at 400 mb will also be shown to compare and contrast to Figs. 1a,b.

As noted earlier, initial vertical motion is determined using the modified balanced omega equation of Krishnamurti (1968). In this study, QG vertical motion is computed at 600 mb, along with PE and IGW vertical motion. The balanced vertical motion used to compute the IGW vertical motion employs the balanced height (geopotential) field that is computed from the analytically determined PE streamfunction at the initial time. Thereafter, a thermodynamic "thickness" equation and

a special equation for the geopotential height of the lowest level are used to obtain the geopotential field at 600 mb. The geostrophic streamfunction ψ_g used in the QG vertical motion calculations is set equal to $f^{-1}\phi$, where ϕ is the geopotential height. The "balanced" streamfunction ψ_B used to compute the balanced vertical motion is computed from the geopotential height field using a balance equation described by Houghton et al. (1981). Vertical motion is set to zero at the top boundary (200 mb) and initially at 1000 mb, also. For each case, the Rossby number, defined as

$$Ro = \frac{|V_{ag}|}{|V|}, \quad (5)$$

is also computed to quantitatively evaluate the degree of ageostrophy of the flow at the initial time. The Rossby number Ro is computed at each grid point to show the spatial variability of the ageostrophy. Since it is extremely sensitive to the actual winds \mathbf{V} , Ro is set to 0 for regions where $|\mathbf{V}| \leq 5 \text{ m s}^{-1}$.

3. Results

a. Initial conditions

Figures 3a–c display the streamfunction and isotachs for the SL, CY, and AC cases at the initial time. As noted earlier, the SL case jet core is 36.0 m s^{-1} , which is 0.4 m s^{-1} greater than the AC case and 1.8 m s^{-1} greater than the CY case. These small differences in the wind maxima at the initial time should have little impact on the vertical motion patterns that evolve, since for each case the downstream change in speed is nearly the same. However, what is emphasized herein is the effect of curvature on the subsequent dynamics.

The initial balanced vertical motions for the SL, CY, and AC jet streaks are shown in Figs. 4a, 4b, and 4c, respectively. For the SL jet streak, we see the classic symmetric, four-cell pattern of UVM in the left-exit and right-entrance regions with DVM in the right-exit and left-entrance regions of the jet.

The CY jet streak shown in Fig. 4b displays equally strong UVM–DVM centers of $\pm 1.5 \mu\text{b s}^{-1}$ about one grid distance (200 km) downstream and upstream from the jet core, respectively. This pattern quantifies the work of Beebe and Bates (1955) for cyclonically curved jet streaks. However, it is important to see that the UVM–DVM cross over to the equatorward side of the jet axis, although the majority of the vertical motion is on the poleward side of the jet axis. The CY jet streak has a vertical-motion magnitude about 2.5 times that of the SL jet streak.

The AC jet streak (Fig. 4c) also reveals a two-cell vertical motion pattern that follows the Beebe and Bates (1955) model. The UVM–DVM regions are about one-third weaker than the CY case and are located about two grid distances (400 km) upstream and downstream from the jet core, respectively. Although the maximum vertical motions are not as strong as in the CY case,

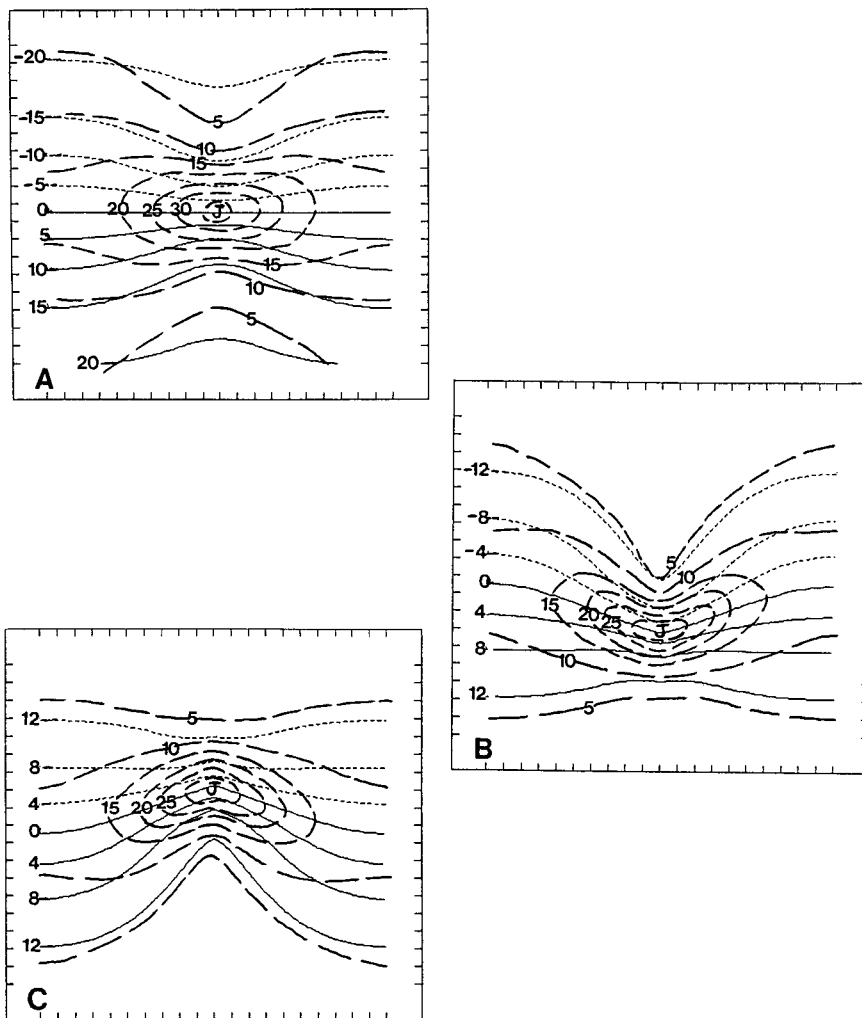


FIG. 3. Streamfunction values ($10^6 \text{ m}^2 \text{ s}^{-1}$), small dashed (negative values) and solid (positive values) lines, and isotachs (m s^{-1} , thick dashed lines) for (a) straight-line jet, (b) cyclonically curved jet, and (c) anticyclonically curved jet. Here J marks the jet core. All values are for the initial time at 400 mb.

one can see that the “10” isopleth covers a broader area than in Fig. 4b. Once again, the vertical motion areas cross over to the opposite side of the jet axis (in this case, poleward). The AC jet streak has vertical motions about 1.6 times that of the SL case.

b. Vertical-motion comparisons

In 12 h, the SL jet streak moves 800 km to the east (Fig. 5a). Although the PE vertical-motion pattern is basically the same as the initial time, the magnitudes of the DVM centers have increased by one-third. The QG vertical motion for this time (Fig. 5b) agrees quite well with the PE vertical-motion pattern. Yet, the UVM–DVM on the equatorward side of the jet axis are considerably weaker than the PE vertical motions. Thus, the QG vertical motions are reasonable approx-

imations to the PE vertical motions on the poleward side of the jet axis but underestimate the PE vertical motion (which approximates truth in this study) significantly on the equatorward side of the jet axis. At 12 h, the SL jet core has decreased to 34.2 m^{-1} , indicating a redistribution of kinetic energy, most likely due to the ageostrophic flow. The increase in the PE vertical motions is probably due to the differential advection of vorticity by the divergent component of the wind (term 10 of Krishnamurti’s balanced omega equation), since the divergent component of the wind has changed the most over the last 12 h.

Although the jet streak is straight-line, there is by necessity a confluent entrance region and a diffluent exit region that create cyclonic (anticyclonic) curvature in the height field to the north (south) of the jet axis.

In this SL jet-streak case, the effect of downstream

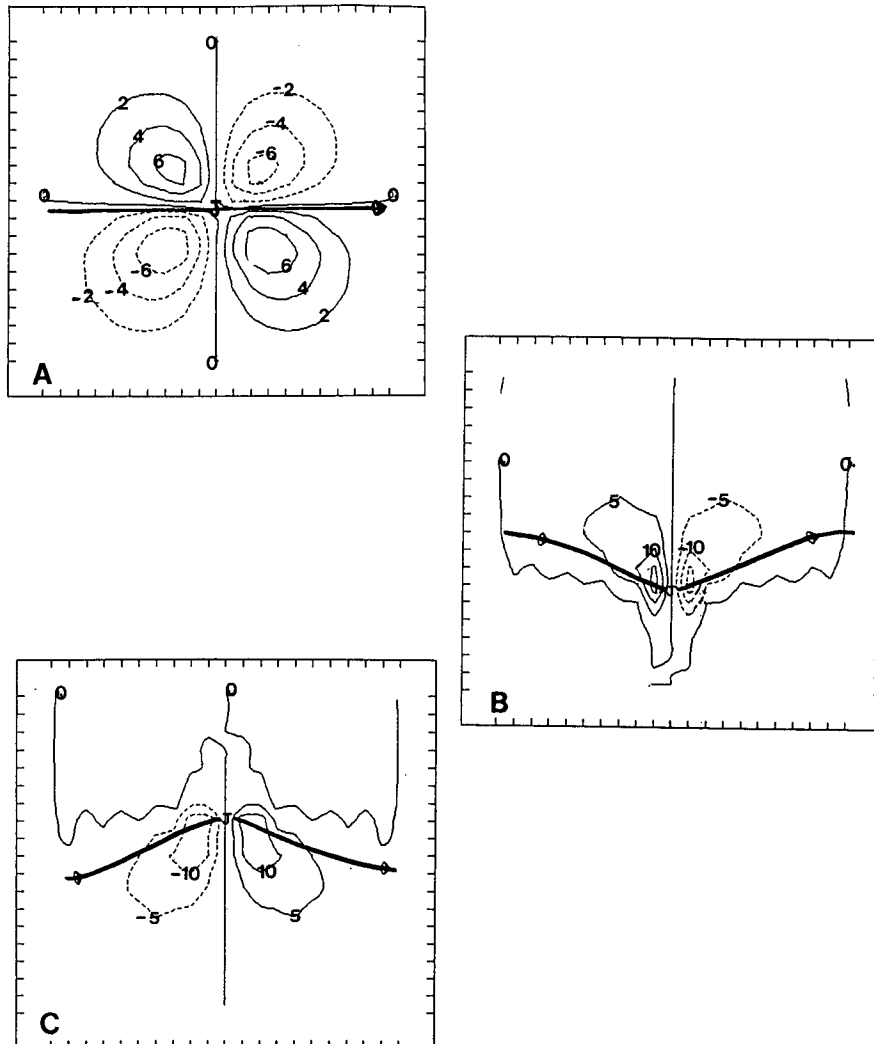


FIG. 4. Vertical motion at 600 mb ($10^{-1} \mu\text{b s}^{-1}$ for all figures) at initial time for (a) straight-line jet, (b) cyclonically curved jet, and (c) anticyclonically curved jet. Here J marks the jet core, and the thick black line is the jet axis.

changes in wind speed creates a northerly ageostrophic wind in the exit region and a southerly ageostrophic wind in the entrance region (Fig. 5c). The effect of alongstream variations in the wind speed on the cross-stream ageostrophic wind dominates the effect of curvature on the ageostrophic flow, as schematically shown in Figs. 1a,b. It is interesting to see, however, that the curvature noted above does slightly enhance the along-stream ageostrophic flow toward the front-right and rear-left quadrants of the jet streak. This increase in the alongstream ageostrophic wind would appear to explain the stronger magnitudes of vertical motion in these quadrants. Note that the stronger wind-speed changes downstream from the jet core result in stronger ageostrophic winds than seen upstream.

The vertical-motion field due to IGWs is shown in

Fig. 5d. As noted by Houghton et al. (1981), this field represents “the unbalanced gravity–inertial component which incorporates both adjustment processes of the large scale and structures with smaller scale energy sources.” Smaller-scale energy sources may include mesoscale perturbation pressure patterns created by diabatic heating and cooling, although such processes are not captured by this model. Thus, we can quantitatively measure the imbalance in the mass–momentum field by examining the IGW vertical motion. Rossby (1938) discussed the formation of IGWs when a rapid increase in momentum was injected into a balanced current. IGWs are a key component of the atmospheric adjustment process (Houghton et al. 1981), since they redistribute mass and momentum in a “disturbed” current. In the case of the SL jet streak at

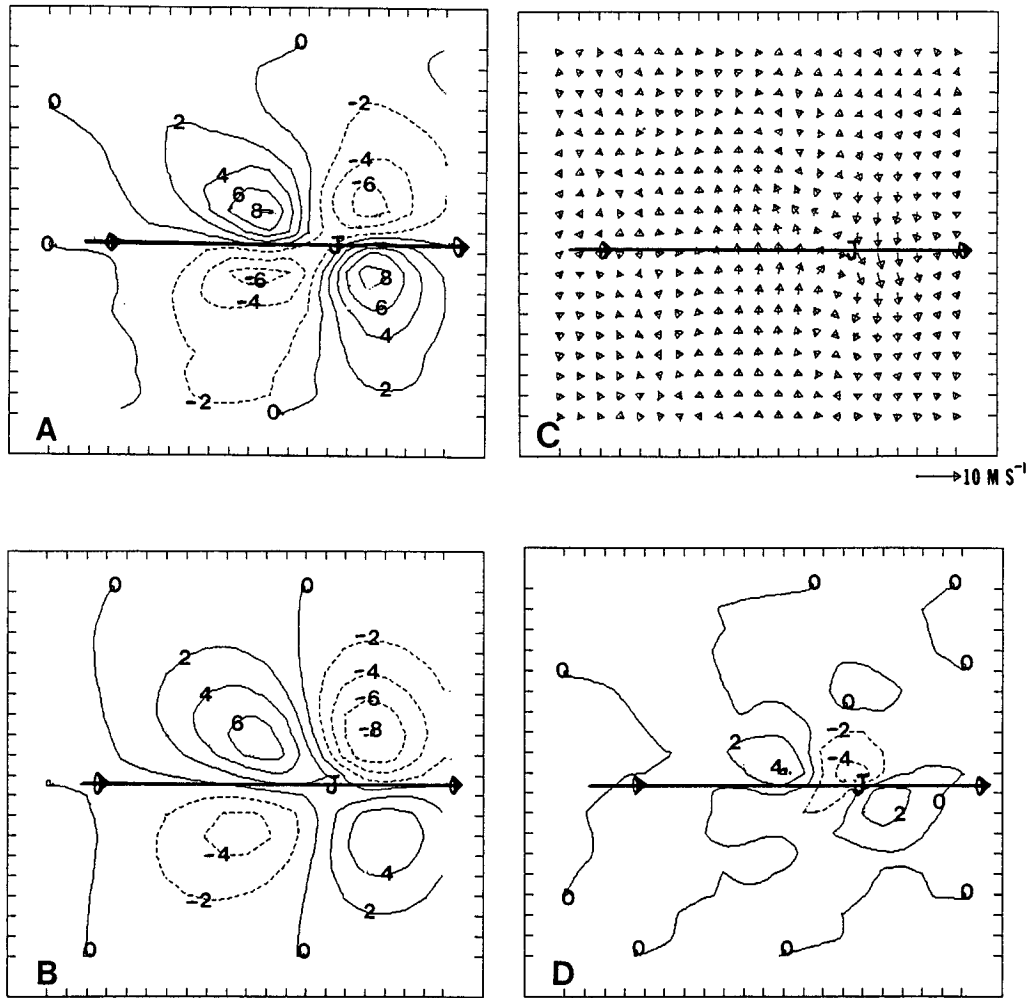


FIG. 5. For the straight-line jet (SL) at 12 h into the simulation for (a) PE vertical motions, (b) QG vertical motions, (c) ageostrophic-wind vectors at 400 mb, and (d) IGW vertical motions. All vertical-motion fields are for 600 mb. Here J marks the jet core, and the thick black line is the jet axis.

12 h, we see a three-cell vertical-motion pattern aligned along the jet streak axis. Magnitudes of the IGW vertical motion are about one-half of the PE vertical motion.

At 12 h, the CY jet streak's PE vertical-motion field (Fig. 6a) has evolved into a five-cell pattern basically aligned along and south of the jet axis. The primary UVM-DVM areas have strengthened by 33% to $2.0 \mu\text{b s}^{-1}$, with the DVM centered about 600 km upstream of the jet core. Three weaker UVM-DVM regions are found further upstream from the jet core in an area where secondary cyclogenesis often takes place, southwest of the major low pressure system at the surface. The primary UVM-DVM maxima are about two times the magnitudes found in the SL jet streak.

Vertical motions associated with cyclonically curved jet streaks tend to be much stronger than those associated with straight-line jet streaks due to the enhanced

divergence-convergence patterns created by the trough-ridge system. Kocin and Uccellini (1990, 42-44) note that "the subgeostrophic flow at the base of the trough and supergeostrophic flow at the crest of the ridge combine to enhance divergence (convergence) downstream (upstream) of the trough axis" (see Fig. 1b). These findings are corroborated by the authors' synoptic experience as well.

The QG vertical-motion pattern for the CY case (Fig. 6b) displays a weaker (by 50%) UVM center compared to the PE vertical motion, while the upstream DVM center compares favorably with the PE vertical-motion value. The two QG vertical motion centers are located about one grid distance (200 km) north of the PE vertical motions. In addition, the QG vertical motions seem to capture the three minor upstream vertical motion cells that appear in the PE vertical motion (Fig. 6a) as seen in the meanders of the zero isopleth on the

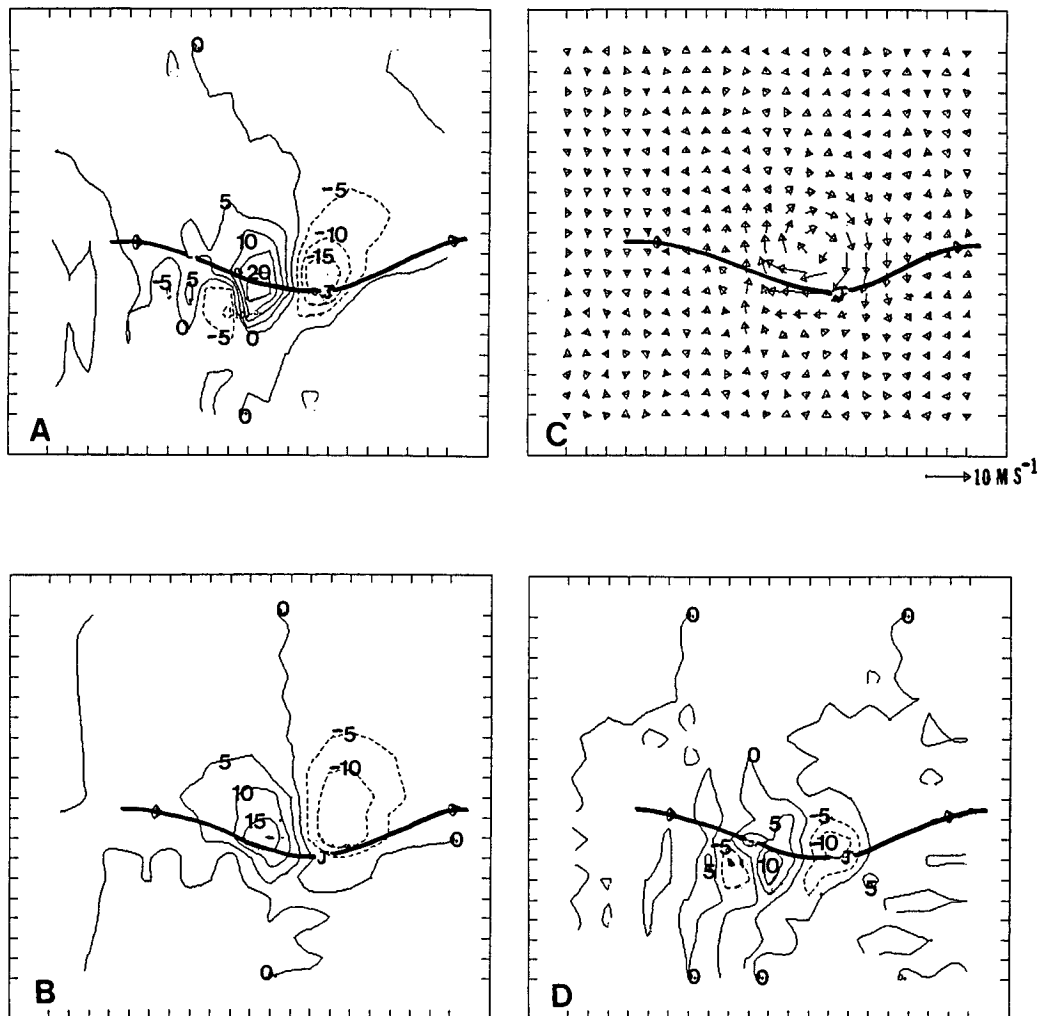


FIG. 6. (a)–(d) Same as Fig. 5a–d except for the cyclonically curved jet streak.

anticyclonic side of the jet axis. However, the amplitude of these features is weaker in the QG result.

The ageostrophic winds at 400 mb (Fig. 6c) for the CY case demonstrate the combined effects of along-stream wind-speed changes and curvature. The anticyclonic gyre of ageostrophic wind vectors, centered about 500 km north of the jet axis, is due to the cross-stream ageostrophic wind being added, vectorially, to the alongstream component of the ageostrophic wind, which is directed upstream due to the cyclonic curvature of the jet streak. This anticyclonic gyre also has a component due to the curvature of the flow away from the jet core. Comparison of Fig. 6c with Fig. 5c reveals that the ageostrophic flow is not only stronger but also more concentrated along the jet-streak axis. Since the ageostrophic flow is easterly and the geostrophic flow is westerly, this implies that the actual flow is *subgeostrophic* along the CY jet core. Undoubt-

edly, this has changed the structure of the vertical motion field so that the UVM–DVM centers are more aligned along the jet rather than across it.

For balanced curved flow (i.e., where the balance vertical motion is a close approximation to the PE vertical motion), we expect the QG vertical motion to be greater than the PE vertical motion. This is expected since the geostrophic wind is an overestimate of the actual wind in cyclonic flow and the vorticity advection scales with the square of the velocity. However, comparing Fig. 6a with Fig. 6b reveals that the PE vertical motions are generally greater than or equal to the QG vertical motions. Noting this, in addition to the fact, which will be discussed later, that the maximum Rossby number for the CY case is about 1.0, leads one to conclude that the flow is considerably unbalanced. This is reflected in the relatively high maximum Rossby number and the strong IGW vertical motions (Fig. 6d).

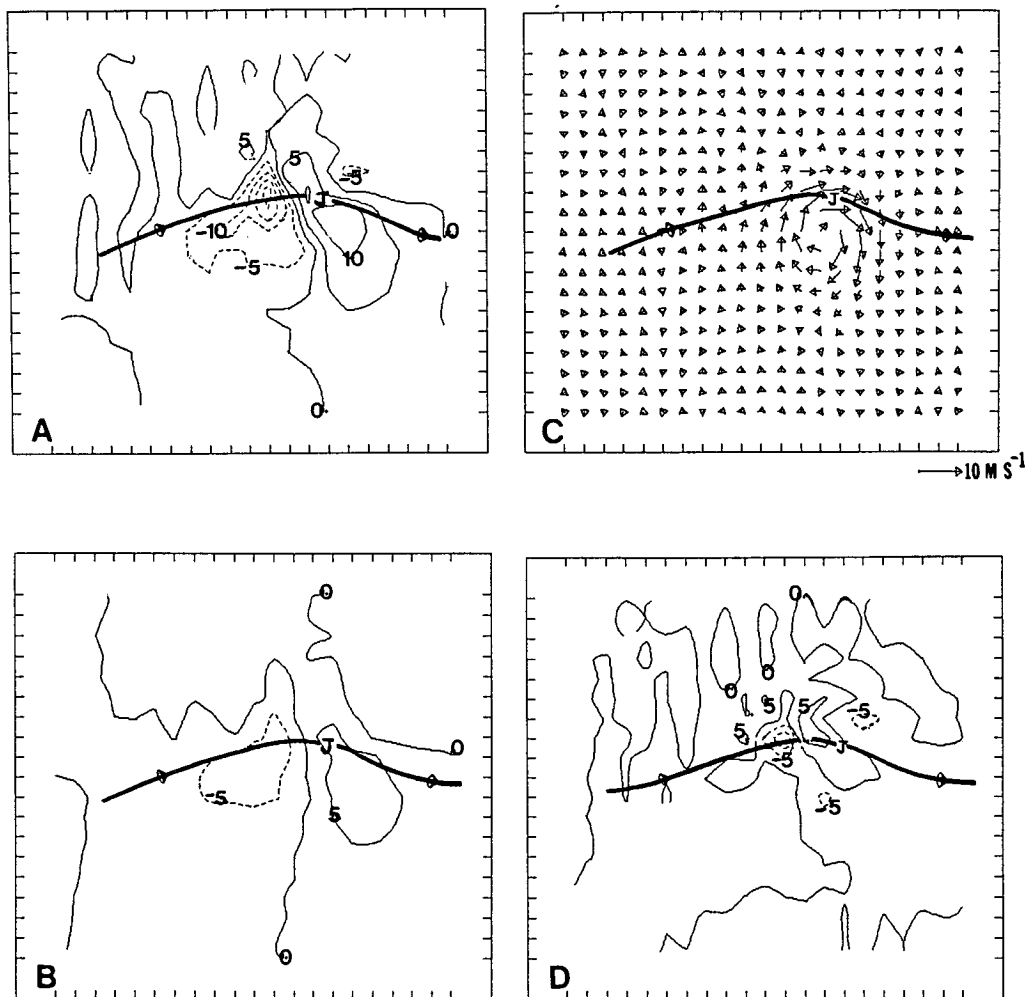


FIG. 7. (a)–(d) Same as Fig. 5a–d except for the anticyclonically curved jet streak.

Thus, there is a considerable component of the flow that can be termed “nongradient” ageostrophic.

The IGW vertical-motion pattern (Fig. 6d) reveals that about one-half of the PE vertical motion can be attributed to the unbalanced flow associated with IGWs. Apparently, two of the three minor UVM–DVM centers located upstream from the jet core are totally due to IGW production. Notice that these IGW vertical motions are nearly two times that for the SL jet-streak case, indicating that a CY jet streak is associated with more of an adjustment process than the SL case. The cyclonic curvature, by creating subgeostrophic winds, increases the mass-momentum imbalance, thereby generating more significant IGW development.

The PE vertical motions for the AC jet streak at 12 h (Fig. 7a) reveal two primary UVM–DVM centers with two weaker cells of $\pm 0.5 \mu\text{b s}^{-1}$ on the poleward side of the jet axis. The primary UVM region is about

600 km upstream from the jet core, while the DVM region is coincident with and downstream from the jet core. The QG vertical motions for this time (Fig. 7b) are much weaker than the PE vertical motions. The QG DVM cell is about 50% of the PE DVM cell, while the QG UVM cell is only about 25% of the PE UVM cell. Also, the QG vertical motions do not show the two minor UVM–DVM centers poleward of the jet axis. Thus, the AC jet streak resulted in weaker QG vertical-motion fields, which greatly underestimated the actual (PE) vertical motion.

The ageostrophic flow for the AC case (Fig. 7c) once again reveals an anticyclonic gyre, only this time it is centered about 500 km *south* of the jet axis. A second major difference between this case and the CY case (Fig. 6c) is that the ageostrophic winds are strongest on the *northern* part of the gyre (top of the ridge) where the flow is westerly. Since the geostrophic flow is also westerly, this implies *supergeostrophic* flow

from the west. This is to be expected in a ridge, as dictated by the relationship between geostrophic and gradient flow. As in the CY case, the significant curvature of the jet axis has increased the curvature effect on the ageostrophic flow, thereby shifting the UVM-DVM centers to a position along the jet axis. A comparison between Figs. 7a and 7b reveals that the QG vertical motions for the AC case are much weaker than the PE vertical motions. This follows from the fact that winds are supergeostrophic in the ridge. The greatest difference is in the PE UVM, which is about four times the QG UVM.

The IGW vertical-motion pattern (Fig. 7d) essentially is similar to the PE vertical motion (Fig. 7a) but about one-half the value along the jet axis. The two minor UVM-DVM cells on the poleward side of the jet axis are IGW induced. The strongest positive-negative vertical-motion couplet is located about 400 km upstream from the jet core along the jet axis. The magnitudes of the IGW vertical motions are slightly higher than those for the SL case. Comparison to the CY case (Fig. 6d) reveals that the IGW vertical motions for the AC case are weaker and cover less of an area. Thus, overall the highest-magnitude IGWs were diagnosed for the CY jet-streak case.

It is interesting to compare the QG vertical motions for each case (Figs. 5b, 6b, and 7b) to the balanced vertical motions. Since most of the difference between these two sets of vertical motion lies in the magnitudes and not the patterns, the results are displayed in Table 1. For the SL jet case, the maximum and minimum values on the poleward (N) and equatorward (S) side of the jet streak are noted.

For the SL jet, the QG vertical motions exceed the magnitude of the balanced vertical motion on the poleward side of the jet where there is weak cyclonic curvature. On the equatorward side of the jet, the balanced vertical motions are slightly stronger than the QG vertical motions due to weak anticyclonic curvature. Differences between the balanced and QG vertical motions are most noticeable in the CY and AC cases. As noted earlier, geostrophic winds exceed the gradient winds in cyclonic curvature, thus QG vertical motions are much stronger than the balanced vertical motion

for the CY case. However, for the AC case, gradient winds are stronger than the geostrophic wind, resulting in much stronger balanced vertical motions than the QG vertical motions. These results bear out the curvature effect on vertical motions most dramatically.

It is also interesting to compare the magnitudes of the balanced and QG vertical motions to the PE vertical motions displayed in Figs. 5a, 6a, and 7a. The QG vertical motions are closer to the PE vertical motions for both the SL and CY cases on the cyclonic-shear side of the jet axis. The QG vertical motions are considerably weaker than the PE vertical motions on the anticyclonic-shear side of the jet axis for the SL case and, to some extent, for the CY case. However, the balanced vertical motions are much closer to the PE vertical motions for the AC case. Thus, one cannot always assume that the balanced vertical motions will necessarily be a better approximation to the PE vertical motions for all jet-curvature types.

Figure 8 summarizes our findings concerning jet-streak curvature and maximum absolute vertical motions at 12 h by presenting 13 runs, 3 of which have been described in detail earlier (see circled X's). Basically, the stronger vertical motions tend to be associated with the CY jet streaks, while AC jet streaks produced stronger vertical motions than the SL jet streaks. The curvature was measured subjectively based on the jet streak, but the overall trend is well defined. It is worth noting that the amount of anticyclonic curvature was limited due to inertial instability. If the AC curvature was increased too much, absolute vorticity on the equatorward side of the jet became negative and inertial instability created large vertical motions in the model. The cyclonic jet streak has no such limit on its curvature.

Figures 9a-c display Ro at 400 mb defined in (5) at the initial time for the SL, CY, and AC jet streaks. For the SL jet streak (Fig. 9a), the maximum Ro is 0.12. This value of Ro is distributed almost symmetrically in the four quadrants of the jet. Minimum values of Ro are found in the jet core since wind speeds are a maximum there. For the CY jet streak (Fig. 9b), a maximum Ro of 1.0 appears about 4.5 grid points (900 km) on the poleward side of the jet axis. For the AC jet streak (Fig. 9c), a maximum Ro of 0.40 appears about 4.5 grid points (900 km) on the equatorward side of the jet core. Thus, in these simulations, cyclonic curvature is more effective in increasing ageostrophy than anticyclonic curvature.

TABLE 1. Comparison of QG vertical-motion and balanced vertical-motion maximum-minimum values for the three jet-streak cases at 12 h.

Jet	Balanced vertical motion		QG vertical motion	
	Maximum	Minimum	Maximum	Minimum
SL	N: +4 S: +6	-4 -4	N: +6 S: +4	-8 -4
CY	+12	-10	+20	-14
AC	+12	-10	+6	-6

4. Conclusions

The PE, QG, and IGW vertical motions were compared for jet streaks of similar magnitudes but with varying curvatures using a simple two-layer PE model. In summary, we found the following held true.

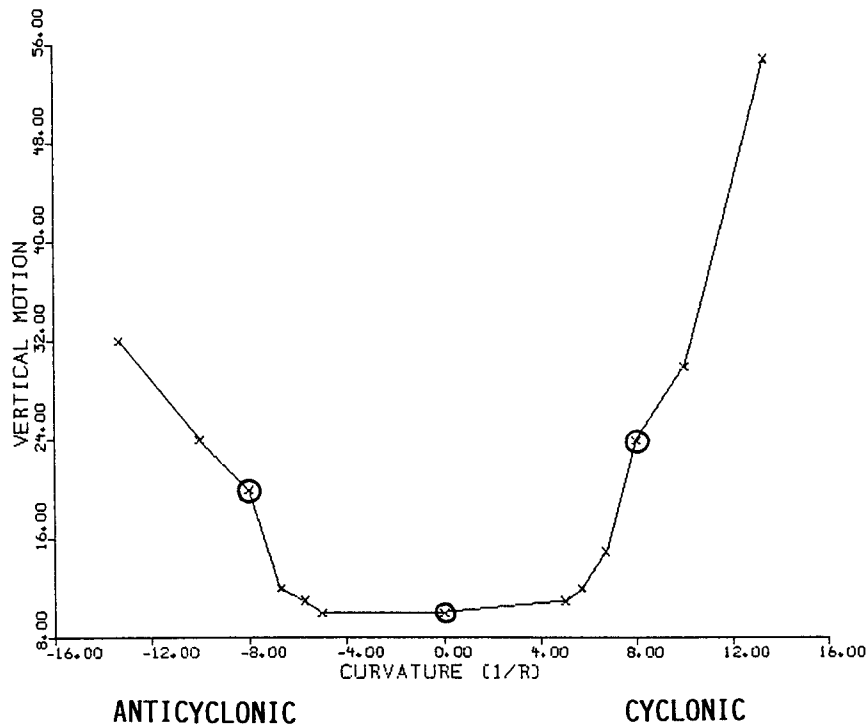


FIG. 8. Maximum vertical motion ($10^{-1} \mu\text{b s}^{-1}$) versus curvature (10^{-7}m^{-1}) at 12 h for 36m s^{-1} jet streaks. Circled X's indicate the three cases discussed in the text.

1) For the initial time period, a two-cell vertical-motion pattern was associated with the CY and AC jet streaks, as opposed to the classic four-cell pattern typically seen with SL jet streaks. Additionally, the vertical-motion centers were oriented more along the jet axis in the curved jets than in the SL jet.

2) The QG vertical motions agreed well with the PE vertical motions for the SL case but were weaker on the equatorward side of the jet axis. For the CY case, the QG UVM was considerably weaker than the PE UVM; however, the QG DVM compared favorably to the PE DVM. The QG vertical motions for the AC case were much weaker than the PE vertical motions.

3) The alongstream ageostrophic wind played an important role in both the CY and AC jet-streak cases. In the CY case, easterly ageostrophic winds resulted in subgeostrophic winds, while in the AC case, westerly ageostrophic winds in the ridge resulted in supergeostrophic flow. In both cases, anticyclonic gyres of ageostrophic winds are associated with stronger UVM-DVM cells that are aligned more along the jet axis rather than across it.

4) IGW vertical motions were strongest for the CY case, where values were about one-half of the PE vertical motions. For the SL and AC cases, IGW vertical motions were smaller but still a substantial part of the total PE vertical motions. It is interesting, however, that the *relative* magnitude of the imbalance is about

50% for all three cases. These results indicate that there is greater mutual adjustment between the mass and momentum fields in jet streaks with cyclonic curvature. The magnitude of the IGW vertical motion is a measure of the nongradient ageostrophic flow contributing to divergence in upper levels.

5) A comparison of the balanced vertical motions to the QG vertical motions revealed the effects of curvature most dramatically. For the SL jet, QG vertical motions exceeded balanced vertical motions on the poleward side (cyclonic curvature) of the jet but were weaker on the equatorward side (anticyclonic curvature). For the CY jet, QG vertical motions were almost 50% stronger than the balanced vertical motions. For the AC jet, QG vertical motions were almost half as strong as the balanced vertical motions. The QG vertical motions were closer to the PE vertical motion magnitudes for both the SL and CY jet cases than to the balanced vertical motions on the cyclonic-shear side of the jet axis. However, on the anticyclonic-shear side of the jet axis, QG vertical motions were substantially less than the PE vertical motions, especially in the SL case. Balanced vertical motions better approximated the PE vertical motions for the AC jet case than the QG vertical motions.

6) The magnitude of the maximum vertical motion accompanying a jet streak is a function of the degree of curvature; this can also be objectively measured via

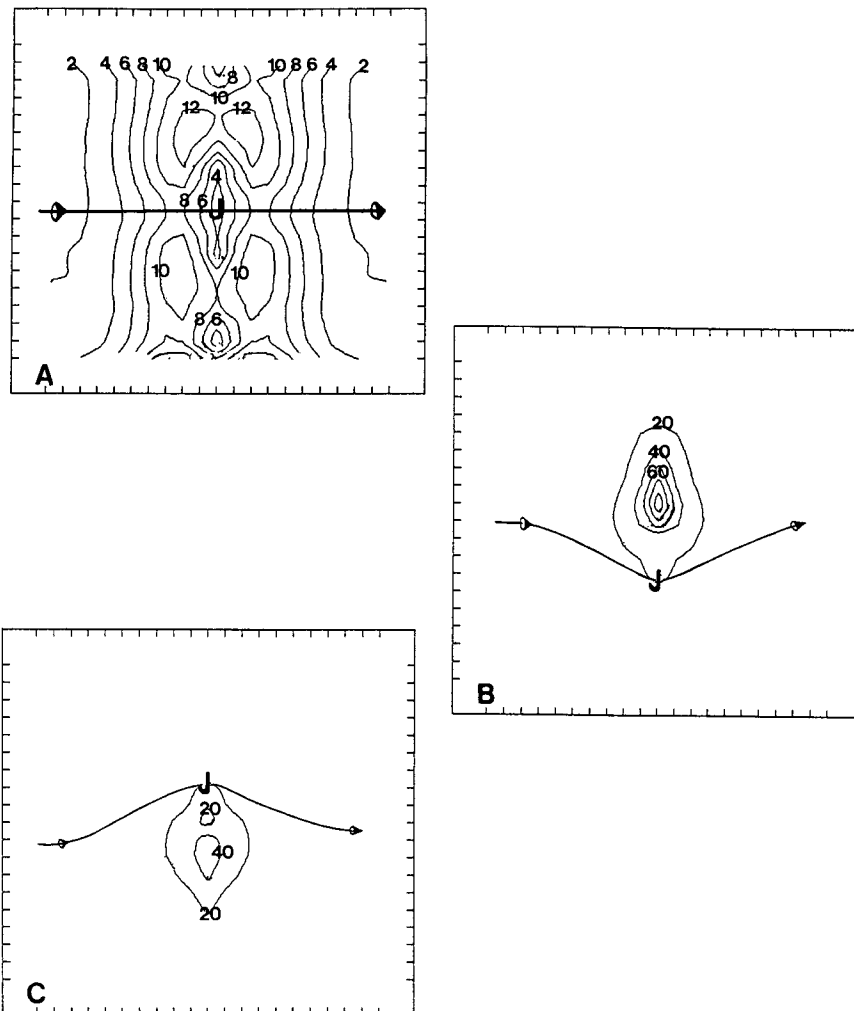


FIG. 9. Rossby numbers (10^{-2}) at 400 mb for (a) straight-line jet, (b) cyclonically curved jet, and (c) anticyclonically curved jet at initial time. Here J marks the jet core, and the thick black line is the jet axis.

the Rossby number. Vertical motion is strongest with cyclonically curved jet streaks, more modest with anticyclonically curved jet streaks, and weakest with straight-line jet streaks. Maximum Rossby numbers were highest (1.00) for the cyclonic jet streak, moderate (0.40) for the anticyclonic jet streak, and weakest (0.12) for the straight-line jet streak, indicating the degree of ageostrophy present in each case.

Acknowledgments. The authors would like to thank Dr. Andrew Van Tuyl of NCAR for providing access to the University of Wisconsin PE model. Drs. G. V. Rao and Larry Coy are appreciated for their help in understanding the model physics and interpreting the model output. James Whistler is thanked for his help

in running the model and programming. Mr. Van-Knowe is appreciative of the Air Force Institute of Technology (AFIT), which supported his M.S. research including this work. Finally, the critical comments of two anonymous reviewers significantly improved the text.

REFERENCES

- Barnes, S. L., 1985: Omega diagnostics as a supplement to LFM/MOS guidance in weakly forced convective situations. *Mon. Wea. Rev.*, **113**, 2122–2141.
- , 1987: Analysis of quasi-geostrophic forcing during the AIMCS project. Volume I: Discussion. NOAA Tech. Memo ERL ESG-27, 31 pp. [Available from National Technical Information Service, 5285 Port Royal Road, Springfield, VA 22161.]

- Beebe, R. G., and F. C. Bates, 1955: A mechanism for assisting in the release of convective instability. *Mon. Wea. Rev.*, **83**, 1–10.
- Cammas, J.-P., and D. Ramond, 1989: Analysis and diagnosis of the composition of ageostrophic circulations in jet-front systems. *Mon. Wea. Rev.*, **117**, 2447–2462.
- Holton, J. R., 1979: *An Introduction to Dynamic Meteorology*. Academic Press, 391 pp.
- Houghton, D. D., W. H. Campbell, and N. D. Reynolds, 1981: Isolation of the gravity–inertial motion component in a nonlinear atmospheric model. *Mon. Wea. Rev.*, **109**, 2118–2130.
- Keyser, D. A., and M. A. Shapiro, 1986: A review of the structure and dynamics of upper-level frontal zones. *Mon. Wea. Rev.*, **114**, 452–499.
- Kocin, P. J., and L. W. Uccellini, 1990: *Snowstorms along the Northeastern Coast of the United States: 1955 to 1985*. *Meteor. Monogr.*, **22**, Amer. Meteor. Soc., 280 pp.
- Krishnamurti, T. N., 1968: A diagnostic balance model for studies of weather systems of low and high latitudes Rossby number less than 1. *Mon. Wea. Rev.*, **96**, 197–207.
- Rosby, C. G., 1938: On the mutual adjustment of pressure and velocity distributions in certain simple current systems, II. *J. Mar. Res.*, **1**, 239–261.
- Shapiro, M. A., and P. J. Kennedy, 1981: Research aircraft measurements of jet stream geostrophic and ageostrophic winds. *J. Atmos. Sci.*, **38**, 2642–2652.
- Shuman, F. G., 1957: Numerical methods in weather prediction II. Smoothing and filtering. *Mon. Wea. Rev.*, **85**, 357–361.
- Uccellini, L. W., and D. R. Johnson, 1979: The coupling of lower tropospheric jet streaks and implications for the development of severe convective storms. *Mon. Wea. Rev.*, **107**, 682–703.
- Van Tuyl, A. H., and J. A. Young, 1982: Numerical simulation of nonlinear jet streak adjustment. *Mon. Wea. Rev.*, **110**, 2038–2054.